論文の内容の要旨

論文題目 Optical detection of symmetry breakings in ferroic materials

(光学現象を利用した強的秩序物質における対称性の破れの検出)

氏　　名 林田　健志

Introduction

Ferroic ordering, which refers to the spontaneous ordering of physical properties in materials, has attracted significant interest in solid state physics. Ferroic ordered states are characterized by symmetry breaking, which induces optical phenomena unique to each type of order. Such optical phenomena allow the detection of ordered states, even in some unconventional ferroic systems where macroscopic properties, such as magnetization or electric polarization, are not observable. Furthermore, spatial distribution measurements of these optical phenomena can reveal how the order parameters are aligned in a sample, i.e., domain structures. In this study, we investigate three different types of ferroic orders: ferrochiral, ferroaxial, and ferromonopolar order, utilizing optical properties unique to each ordered state.

Ferrochiral order

Chirality, which describes the asymmetry of an object upon its mirroring, is ubiquitous in materials and has long been of considerable interest in various fields of science [1]. However, it has not been widely recognized as a ferroic property. This is possibly because there are only a few materials which exhibit an achiral-chiral transition (ferrochiral transition), where chirality is a primal order parameter. Here, we investigate the ferrochiral order in one of the few such examples, $Ba(TiO)Cu_4(PO_4)_4$ (BTCPO).

BTCPO undergoes a structural phase transition from a low-temperature (T) chiral phase (space group: $P42_12$) to a high-T achiral phase (space group: $P4/nmm$) at T_c = 710 °C [2]. This transition is characterized by a staggered rotation of antipolar Cu_4O_{12} units, as shown in Fig. 1**a**. In the chiral phase, a pair of domain states with opposite handedness (levo and dextro) coexist. The mirror symmetry breaking in chiral compounds induces natural optical rotation (OR), that is, rotation of polarization plane of transmitted light. The direction of OR is opposite between the opposite handedness domains, and thus spatial distribution measurements of OR will visualize chiral domain structures.

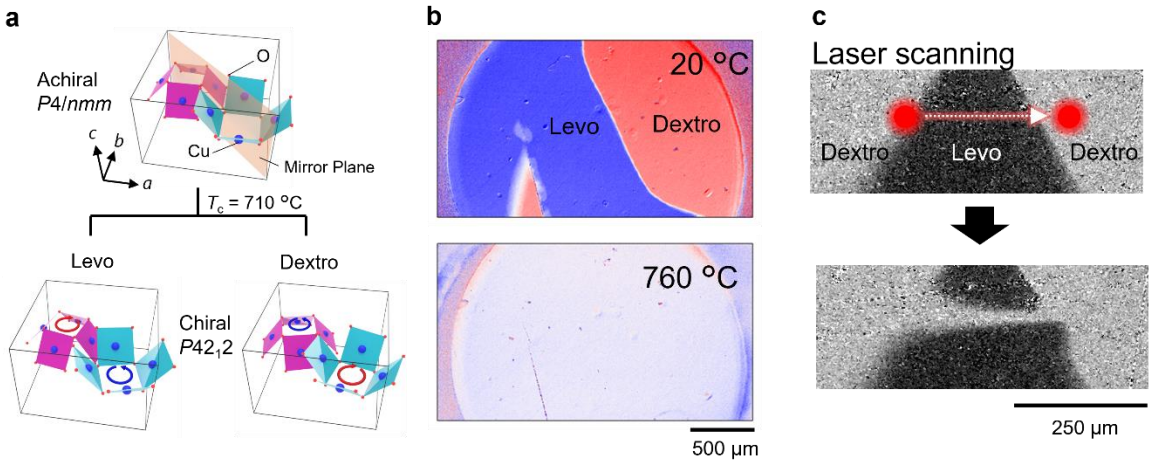

Fig 1 Ferrochiral transition and ferrochiral domains in $Ba(TiO)Cu_4(PO_4)_4$ **a**, Schematic crystal structures in the achiral (top) and chiral (bottom) phases. Only Cu and O atoms are depicted. **b**, Ferrochiral domains observed by spatial distribution measurements of optical rotation. At 760 °C (> T_c), domain contrasts disappear. **c**, Laser writing of a chiral domain pattern. Top and bottom panels show the domain patterns before and after laser scanning, respectively.

We measured temperature dependence of spatial distributions of OR in a single crystalline sample of BTCPO. As a result, we successfully visualized a temperature evolution of ferrochiral domains across T_c (Fig. 1**b**). After the characterization of the ferrochiral order, we tried chirality switching in BTCPO. Unlike an electric field for ferroelectric materials and stress for ferroelastic materials, there is no simple conjugate field to switch chirality, making chirality control difficult. In this work, we demonstrate chirality switching by manipulating the domain boundaries with laser irradiation. Local heating induced by laser irradiation leads to reconstructions of chiral domain boundaries. In this reconstruction process, energetically unstable domain boundaries tend to be minimized, which affects resultant domain patterns. Based on this feature, we successfully manipulate chiral domains by scanning the laser beam on the sample surface (Fig. 1**c**).

Ferroaxial order

Ferroaxial order is a new class of ferroic order characterized by a spontaneous rotational distortion [3,4]. Such a rotational distortion in a crystal can be regarded as a head-to-tail arrangement of electric dipole moment, and the order parameter of the ferroaxial order is the ferroaxial moment **A** (sometimes called electric toroidal moment), defined as $\mathbf{A} \propto \sum_i \mathbf{r}_i \times \mathbf{p}_i$. Here, $\mathbf{r}_i$ is a position vector of an electric dipole moment $\mathbf{p}_i$ at i site. **A** is a time-even axial vector, and it is invariant to time reversal and space inversion operations. Instead, it breaks the mirror symmetry whose mirror plane includes the rotation axis. Thus, in the ferroaxial ordered state, a pair of the two domain states with the opposite signs of **A** coexist.

Due to its high symmetry, observation of ferroaxial order with identifying the sign of **A** is non-trivial. In 2020, the presence of ferroaxial domains was experimentally confirmed in $RbFe(MoO_4)_2$, which is one of the representative ferroaxial materials, by using rotational anisotropy second harmonic generation [5]. However, spatial distributions of ferroaxial domains were not observed. In this work, we visualize ferroaxial domains in two representative ferroaxial materials, $NiTiO_3$ and $RbFe(MoO_4)_2$, by using the so-called linear electrogyration (EG), that is, electric-field-induced optical rotation. Between the two domain states with the opposite signs of **A**, the direction of EG will be opposite [6]. Therefore, ferroaxial domains can be visualized by spatial distribution measurements of EG.

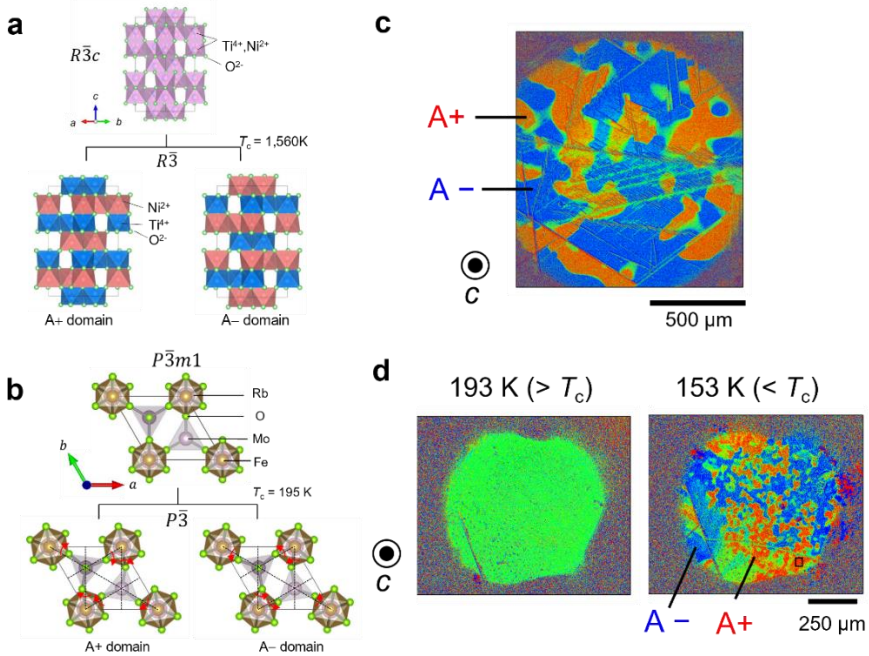

Fig. 2 Ferroaxial transition and ferroaxial domains in $NiTiO_3$ and $RbFe(MoO_4)_2$. **a**, Crystal structures of $NiTiO_3$ in the non-ferroaxial (top) and ferroaxial (bottom) phases. **b**, Crystal structures of $RbFe(MoO_4)_2$ in the non-ferroaxial (top) and ferroaxial (bottom) phases. **c**. Ferroaxial domains observed in $NiTiO_3$. **d**. Ferroaxial domains observed in $RbFe(MoO_4)_2$. At 193 K (> T_c), domain contrasts disappear.

$NiTiO_3$ undergoes an order-disorder type phase transition from a low-T ferroaxial phase (space group: $R\bar{3}$) to a high-T non-ferroaxial phase (space group: $R\bar{3}c$) at T_c = 1560 K [7]. On the other hand, $RbFe(MoO_4)_2$ undergoes a displacive type phase transition from a low-T ferroaxial phase (space group: $P\bar{3}$) to a high-T non-ferroaxial phase (space group: $P\bar{3}m1$) at T_c = 190 K [5]. In these two materials, we obtained two-dimensional maps of EG using a polarized microscope by applying a field-modulation-imaging technique [8]. In $NiTiO_3$, ferroaxial domains were observed only at room temperature, but in several single crystalline samples which were grown in different methods and annealed in different conditions. In $RbFe(MoO_4)_2$, spatial distribution measurements of EG were performed at several temperatures across T_c to observe how domains are formed and how the magnitude of EG behaves with changing temperature.

Figure 2 shows the representative results. Both in $NiTiO_3$ and $RbFe(MoO_4)_2$, ferroaxial domains were clearly visualized. In $NiTiO_3$, by comparing the obtained domain structures in different samples, we found some characteristics of domain formation, such as a cooling rate dependence of domain sizes. In $RbFe(MoO_4)_2$, the temperature profiles of EG were well fitted by the function of the order parameter in the first-order transition, which confirms the effectiveness of EG measurements to observe the evolution of ferroaxial order.

In $NiTiO_3$, we also investigate another unique optical property, electric-field-induced magnetochiral dichroism (*E*-MChD). MChD is an asymmetry in the absorption of two counter propagating unpolarized electromagnetic waves in magnetized chiral compounds [9]. In ferroaxial materials, chirality can be induced by applying an electric field, and thus such an asymmetry in the absorption is expected to be observed under the simultaneous application of an electric field (**E**) and a magnetic field (**H**).

We performed spectroscopy measurements of *E*-MChD in near-infrared regions by taking a difference of absorption coefficients obtained with and without electric and magnetic fields. As a result, *E*-MChD was observed around the excitation energy corresponding to Ni^{2+} *d-d* magnetic-dipole transitions. The result is nicely explained by adopting the theory of MChD concerning the pseudo-Stark splitting of the energy states.

Ferromonopolar order

In the antiferromagnetic (AFM) ordered state, the net magnetization is canceled out, which usually makes the observation of AFM domains difficult. However, in some classes of antiferromagnets in which AFM ordering breaks both the time-reversal and space-inversion symmetries, unique nonreciprocal optical effects are induced due to the linear magnetoelectric (ME) coupling, which can be utilized to distinguish AFM domain states. Here, we demonstrate the observation of AFM domains in the archetypal ME antiferromagnet Cr_2O_3, whose magnetic structure can be classified as ferromonopolar order, using three different types of nonreciprocal optical effects.

Cr_2O_3 shows a ferromonopolar AFM ordering at temperatures below $T_N \approx 307$ K [10]. The magnetic symmetry in this AFM phase is $\bar{3}'m'$, which allows the diagonal ME effects with nonzero ME tensor components of $\alpha_{11} = \alpha_{22}$ and α_{33} [11]. Here α_{ij} is the linear ME tensor which describes the linear ME coupling as $P_i = \alpha_{ij}H_j$ ($\mu_0 M_i = \alpha_{ij}E_j$), where P is electric polarization, M is magnetization and μ_0 is the permeability of vacuum. A pair of domain states (L+ and L-), which is related by either time reversal or space inversion, develops in the AFM phase.

The diagonal components of α_{ij} contribute to unconventional nonreciprocal optical effects. Here we focus on the following three effects. The first one is the electric-field-induced (*E*-induced) Faraday effect [12]. It refers to the polarization rotation of transmitted light induced by applying an electric field. Cr_2O_3 exhibits the *E*-induced Faraday effect when an electric field is applied (anti)parallel to the light propagation direction. This effect is intuitively understood considering that magnetization is induced in the same direction with an applied electric field. Like the magnetic circular dichroism, which is a counterpart of the Faraday effect related by the Kramers-Kronig relation, Cr_2O_3 will also exhibit the electric field induced magnetic circular dichroism (*E*-induced MCD). Another nonreciprocal optical effect is the nonreciprocal rotation of reflected light (NRR) [13]. NRR derives from the diagonal components of α_{ij} expanded to optical frequencies, and polarization rotation angle θ in geometry $\mathbf{k} \parallel c$ is given by $\theta = 2\,\mathrm{Re}[\alpha_\perp(1+n_\perp)/(1-n_\perp)]$. Here, $\alpha_\perp = \alpha_{11}(\omega) = \alpha_{22}(\omega)$ is the ME coefficients expanded to the optical frequencies and $n_\perp^2 = \epsilon_{11}(\omega) = \epsilon_{22}(\omega)$

is the dielectric constant.

Because the signs of the above-mentioned optical effects will be opposite between the L+ and L- domain states (see the top panels in Fig. 3), they are useful to visualize AFM domains in Cr_2O_3. However, such a domain imaging has not been reported to date, most likely because these effects are relatively small.

In this work, first we measure spectra of the *E*-induced Faraday effect and *E*-induced MCD in the visible light region, and demonstrate that Cr_2O_3 exhibits large enhancements at wavelengths around the spin allowed *d-d* transitions. Next, we successfully visualize AFM domains of Cr_2O_3 using the *E*-induced Faraday effect, *E*-induced MCD, and NRR (see bottom panels in Fig. 3), by adopting the electric-field modulation imaging [8] and the polarization modulation imaging [14].

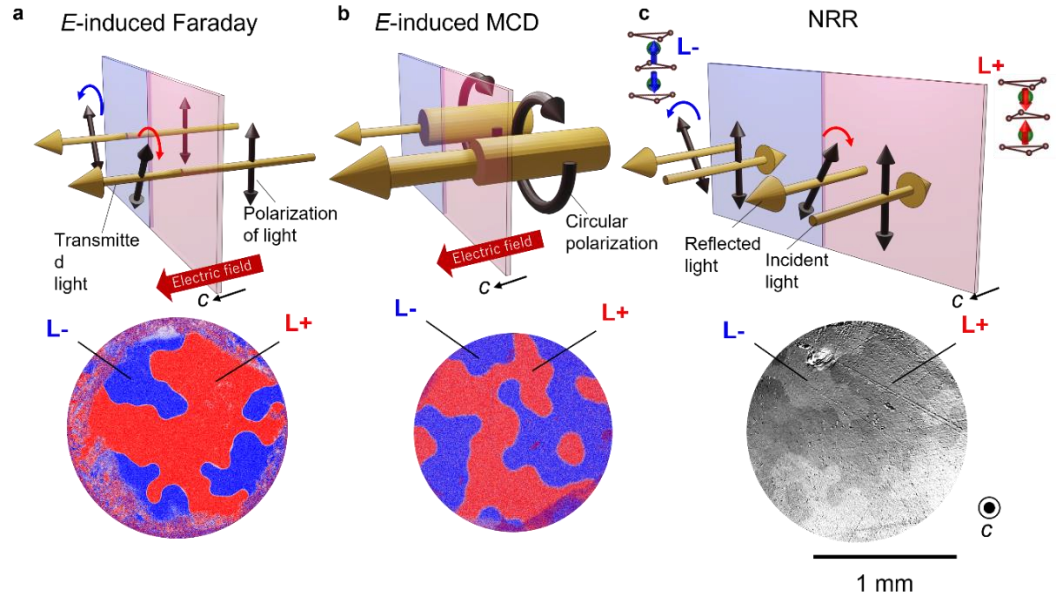

Fig. 3 AFM domain observation in Cr_2O_3 via nonreciprocal optical effects. **a**, Electric-field-induced (*E*-induced) Faraday effect. **b**, *E*-induced magnetic circular dichroism (*E*-MCD). **c**, Nonreciprocal rotation of reflected light (NRR). The top panels show conceptual diagrams of each effect, and the bottom panels show the obtained domain images.

Conclusion

In summary, we successfully observed the optical effects induced by characteristic symmetry breakings in the three different types of ferroic orders: ferrochiral, ferroaxial, and ferromonopolar orders. In particular, domain images were obtained in all types of ferroic materials by measuring the spatial distribution of the optical effects. Our achievements in this work show that the symmetry-sensitive optical effects are powerful tools for detecting ferroic orders, and will further promote the research on ferroic orders.

References

[1] L. D. Barron, *Chem. Soc. Rev.* **15**, 189 (1986). [2] K. Kimura *et al*., *Inorg. Chem.* **55**, 1002 (2016). [3] R. D. Johnson *et al., Phys. Rev. Lett.* **107**, 137205 (2011). [4] J. Hlinka *et al*., *Phys. Rev. Lett.* **116**, 117602 (2016). [5] W. Jin *et al*., *Nat. Phys.* **16**, 42 (2020). [6] S. -W. Cheong *et al*., *npj Quantum Mater.* **3**, 19 (2018). [7] M. Lerch *et al., J. Phys. Chem. Solids* **53**, 1153 (1992). [8] Y. Uemura *et al*., *Phys. Rev. Appl.* **11**, 014046 (2019). [9] G. L. J. A. Rikken and E. Raupach, *Nature* **390**, 493 (1997). [10] T. R. McGurie *et al*., *Phys. Rev.* **102**, 1000 (1956). [11] E. Kita *et al., Jpn. J. Appl. Phys.* **18**, 1361 (1979). [12] T. H. O'Dell and E. A. D. White, *Philos. Mag. A J. Theor. Exp. Appl. Phys.* **22**, 649 (1970). [13] R. M. Hornreich and S. Shtrikman, *Phys. Rev.* **171**, 1065 (1968). [14] T. Ishibashi *et al., J. Appl. Phys.* **100**, 093903 (2006).